JOURNAL OF CATALYSIS 23, 321–330 (1971)

Hydrogen Exchange Rates on Nickel by Chromatography

MOTOYUKI SUZUKI* AND J. M. SMITH

University of California, Davis, California 95616

Received February 26, 1971; accepted May 5, 1971

A method of measuring exchange rates by isotope chromatography is described and then used to study exchange of hydrogen on a nickel/kieselguhr catalyst. Adsorption isotherms and rates were obtained at 24 to −30°C and for hydrogen pressures from 40 to 780 mm Hg.

The results showed that the available sites at each temperature were nearly saturated with hydrogen over the entire pressure range. The exchange rate was approximately one-half order with respect to hydrogen.

NOMENCLATURE

C	concentration in gas phase, mole/cm³
D_e	intraparticle diffusivity, cm²/min
$\mathfrak{D}$	molecular diffusivity in gas phase, cm²/min
E_A	axial dispersion coefficient, based on cross-sectional area of empty tube, cm²/min
E	apparent activation energy; kcal/mole
H	function of moments defined by Eq. (18), min
H_0	value of H at $1/v = 0$, min
k^*	pseudo-rate constant, defined by Eq. (11), cm³/(g)(min)
K^*	pseudo-equilibrium constant defined by Eq. (12), cm³/g
k	apparent adsorption, or exchange, rate constant
K_e	adsorption equilibrium constant, (mm)⁻¹
k_f	fluid-to-particle surface mass transfer coefficient, cm/min
n	amount adsorbed on catalyst surface, mole/(g of reduced catalyst)
p_H	hydrogen pressure, mm Hg
q	isosteric heat of adsorption, kcal/mole
R	exchange rate of hydrogen, mole/(min)(g of reduced catalyst)
R_g	gas constant
r_0	average radius of particles (assumed to be spherical), cm
T	temperature, °K
t	time, min
v	interstitial velocity of gas, cm/min
z	length of the bed of particles, cm

Greek Letters

α	void fraction in the bed
β	intraparticle porosity
δ_0, δ_1	defined by Eqs. (20) and (21)
ρ_p	particle density, g/cm³
μ	moment
θ	fraction of available sites occupied by hydrogen

Subscripts

a, d	adsorption, desorption
eff, in	corresponds to effluent and inlet streams to bed of particles
1, 2	first and second moments
D, H, t	deuterium, hydrogen, and total
I, II, III	mechanisms I, II, or III

Chemisorption of hydrogen on nickel catalysts has been extensively studied and summaries are available (*1–4*). Three mechanisms have been proposed for the exchange

* On leave from Institute of Industrial Science, University of Tokyo.

of hydrogen between the gas phase and the nickel surface:

I. Bonhoeffer–Farkas,

$$H_2 + 2 \cdot S \rightleftharpoons 2\, H \cdot S$$

II. Rideal–Eley, single site,

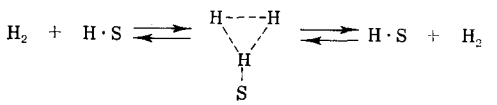

III. Rideal–Eley, two-site,

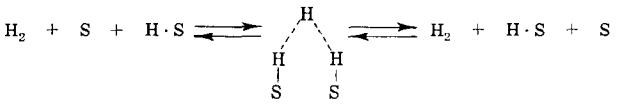

The three mechanisms are distinguishable through the pressure dependence on the rate. Following Langmuir postulates, the rates of adsorption and desorption for I are:

$$R_a = k_a p_H (1 - \theta)^2, \quad (1)$$

$$R_d = k_d \theta^2, \quad (2)$$

where θ and p_H are the fraction of available sites occupied by hydrogen atoms and the partial pressure of hydrogen molecules in the gas. For mechanisms II and III the exchange rates are

$$R = k_{II} p_H \theta \quad (3)$$

and

$$R = k_{III} p_H \theta (1 - \theta). \quad (4)$$

The adsorption isotherm, from Eq. (1) and (2), is

$$\frac{k_a}{k_d} p_H (1 - \theta)^2 = \theta^2.$$

At nearly saturated conditions ($\theta \approx 1$), this reduces to

$$1 - \theta = \left(\frac{k_a}{k_d} p_H\right)^{-1/2}. \quad (5)$$

Combining Eq. (5) with Eqs. (1–4) to eliminate $(1 - \theta)$ gives the exchange rate for each mechanism in a form which shows the different dependences upon the hydrogen pressure:

$$\text{I.} \quad R = R_a = R_d = k_d \quad (6)$$

$$\text{II.} \quad R = k_{II} p_H \quad (7)$$

$$\text{III.} \quad R = k_{III} p_H^{1/2} \left(\frac{k_d}{k_a}\right)^{1/2} = \frac{k_{III}}{(K_e)^{1/2}} p_H^{1/2}, \quad (8)$$

where the last form of Eq. (8) is written in terms of the adsorption equilibrium constant, K_e.

Isotope chromatography provides a means for measuring exchange rates at various pressures and thus is useful in mechanism studies. However, the identification of mechanism is not as simple as comparing experimental rate vs pressure data with Eqs. (6–8). Variations in activity (energy configuration) of sites, and the existence of different types of adsorbed hydrogen, as described by Bond (*4*), are some of the factors that complicate the mechanism question. However, surprisingly few measurements have been made of the order of the exchange rate with respect to hydrogen pressure. The major objective of this work is to show how such information can be obtained in a rather simple way by isotope chromatography and to present results for a hydrogen–nickel system.

Isotope Chromatography

If a pulse of deuterium is introduced into the hydrogen stream fed to a bed of catalyst particles, the rate of deuterium exchange between gas and catalyst can be evaluated from the moments of the chromatographic peak of isotope in the hydrogen stream leaving the column. This evaluation requires the separation of the effects of transport processes from the exchange reactions at the adsorption sites. Since the catalyst surface has been exposed to hydrogen long enough to reach equilibrium adsorption, the exchange rate is measured at constant surface conditions.

If the isotope effect on the rate is neglected, the rate of exchange is given by multiplying the total exchange rate by the fraction of deuterium molecules:

$$R_D = R\frac{C_D}{C_t} - R\frac{n_D}{n_t} \quad (9)$$

$$= k^*\left(C_D - \frac{n_D}{K^*}\right), \quad (10)$$

where

$$k^* = R/C_t, \quad (11)$$

$$K^* = n_t/C_t. \quad (12)$$

It is supposed that equilibrium exists for the reaction $H_2 + D_2 \rightleftarrows 2HD$, so that defining C_D as $C_{D_2} + \frac{1}{2} C_{HD}$ will account for all of the deuterium present.

The parameters k^* and K^* are determined by analyzing the moments of the chromatographic peaks, and then the exchange rate R and the amount adsorbed n_t are calculated from Eqs. (11) and (12). The first absolute moment, μ_1, and the second central moment, μ'_2, are obtained from the measured concentration peaks using the equations:

$$\mu_1 = \frac{\int_0^\infty C_D t\, dt}{\int_0^\infty C_D\, dt}, \quad (13)$$

$$\mu'_2 = \frac{\int_0^\infty C_D(t - \mu_1)^2\, dt}{\int_0^\infty C_D\, dt}. \quad (14)$$

The apparatus was arranged so that a pulse of D_2 was introduced into a stream of hydrogen and helium, which then entered one side of a thermal conductivity cell used to determine C_D. Then the mixture flowed through the bed of catalyst particles and on through the other side of the cell. With this arrangement C_D was measured, and μ_1 and μ'_2 calculated from Eqs. (13) and (14), for both the inlet and effluent streams from the bed. In the analysis the moments, $\Delta\mu_1$ and $\Delta\mu'_2$, for the bed itself are needed. They are given by

$$\Delta\mu_1 = (\mu_1)_{eff} - (\mu_1)_{in} - (\Delta t)_{d.\,vol} \quad (15)$$

$$\Delta\mu'_2 = (\mu'_2)_{eff} - (\mu'_2)_{in}, \quad (16)$$

where $(\Delta t)_{d.\,vol}$ is the residence time in the total dead volume between the detector and bed. This volume was reduced to 1.0 cm³ in order to minimize this correction in Eq. (15). At the flow rates used, $(\Delta t)_{d.\,vol}$ was less than 1.3% of $(\mu_1)_{eff}$ for the deuterium runs. Previous studies (*5*) have shown that dispersion in dead volumes of this magnitude, and for the range of velocity used, gave a contribution of less than 3% to the second moment for adsorbable gases. Values of $\Delta\mu_1$ ranged, for the most part, from 1 to 10 min.

The relationships between the moments and the rate constant k^* and pseudo-equilibrium constant K^* for exchange, and the rate constants (E_A, k_f, D_e) for transport processes, already have been developed (*6–8*) for chromatographic experiments. The pertinent results are:

$$\Delta\mu_1 = \frac{z}{v}(1 + \delta_0), \quad (17)$$

$$H = \frac{\Delta\mu'_2}{(\Delta\mu_1)^2}\left(\frac{z}{2v}\right) = H_0 + \frac{1}{v^2}\frac{E_A}{\alpha}, \quad (18)$$

where

$$H_0 = \frac{\delta_1}{(1 + \delta_0)^2}, \quad (19)$$

$$\delta_0 = \frac{1 - \alpha}{\alpha}\beta\left(1 + \frac{\rho_p K^*}{\beta}\right), \quad (20)$$

$$\delta_1 = \frac{1 - \alpha}{\alpha}\beta\left[\frac{\rho_p}{\beta}\frac{(K^*)^2}{k^*} + \frac{r_0^2\beta}{15}\left(1 + \frac{\rho_p K^*}{\beta}\right) \times \left(\frac{1}{D_e} + \frac{5}{k_f r_0}\right)\right]. \quad (21)$$

These equations were used to obtain k^* and K^*, as described later.

Experimental

The apparatus was similar to that employed for studying exchange rates for hydrogen on a Cu·ZnO catalyst and has been described (*6*). A deuterium pulse of 0.3 cm³ was introduced into a pure-hydrogen stream, which was then mixed with helium to obtain the desired partial pressure of hydrogen plus deuterium in the system. The flow rates of the dried (silica-gel beds) helium and hydrogen were measured separately with soap-film meters. The pressure associated with a specific run was taken as the average of the measured pressures at the inlet and outlet of the bed. The maximum Δp was 30% of the outlet pressure (1 atm) but for most runs this figure was

about 5%. The total flow rate was also measured at the outlet of the bed and corrected to the average pressure. The bed consisted of a 0.49 cm i.d. tube packed to a length of 50 cm with catalyst particles.

The hydrogen used had a stated purity of 99.95% and was subsequently passed through a De-oxo unit to remove traces of oxygen. The helium had a stated purity of 99.99% while technical grade deuterium (98% purity) was used.

The catalyst particles were obtained by crushing and sieving nickel/kieselguhr pellets (catalyst G-49B from the Catalysts Division of Chemetron Corporation) which contained 50 wt % Ni in the reduced state. All data were taken with particles having an average radius of 0.114 mm. The void fraction (α) in the bed was calculated from the known particle density (see Table 1)

TABLE 1
PROPERTIES OF CATALYST PARTICLES

Nickel content = 50% (reduced state)	
Apparent particle density[a]	$\rho_p = 1.73$ g/cm^3
Total particle porosity[a]	$\beta = 0.58$
Surface area[a]	$S = 205$ m^2/g (unreduced)
Ni surface area[a]	$S_{Ni} = 42$ m^2/g (unreduced)
Particle size	Diameter range 208–246 μ
Average radius	$r_0 = 0.114$ mm

[a] From Ref. (7).

and the measured mass of reduced catalyst. The particles were reduced *in situ* by flowing hydrogen over the bed at a steadily (1°C/min) increasing temperature and at a rate of 60 cm^3/min until 350°C was reached. Then the hydrogen flow was continued for 10 hr at a temperature of 350°C. The bed was maintained under a hydrogen atmosphere at all times. At intervals of about 50 hr the bed was heated to 350°C, although there was no indication of change in activity before and after this high-temperature cleaning process.

Particles prepared from the same batch of catalyst had been used previously (7) for rate measurements with pure hydrogen, and at that time properties of the reduced catalyst were determined. Some of these results are included in Table 1.

Program of Experiments

First, helium pulses were introduced when pure hydrogen was flowing through the bed at 24°C. Analysis of ($\Delta\mu'_2$) for these helium peaks established the effect of axial dispersion (E_A) and intraparticle diffusivity (D_e). Then deuterium pulses were introduced into pure hydrogen flow with the bed at 24, 0, −10, −20, and −30°C. Measurements of $\Delta\mu_1$ and $\Delta\mu'_2$ for various flow rates (18–370 cm^3/min at 24°C) confirmed axial dispersion effects and provided R and n_t for $p_H \approx 760$ mm. Finally, deuterium pulses were used with a carrier gas consisting of mixtures of helium and hydrogen. Moments for these runs permitted evaluation of R and n_t for $40 < p_H < 780$ mm. During these latter runs the total flow rate was maintained nearly the same for all runs (at about 70 cm^3/min).

First-Moment Analysis

The data for $\Delta\mu'_1$ were used with Eqs. (15), (17), and (20) to calculate K^*. Then n_t was obtained from Eq. (12), taking $C_t = p_H/R_gT$. The results for the five temperatures are plotted vs p_H in Fig. 1. For clarity, data points are not shown for 0 and −20°C, but lines (dotted) representing the data are included. The nearly flat lines indicate that the surface is close to saturation with adsorbed hydrogen at pressures down to 40–60 mm. The values at 780 mm agree well with the data of Padberg (7) for the same catalyst, as shown in the upper half of Fig. 2.

The isosteric heat of adsorption was estimated from the isotherm data in Fig. 1 using the equation

$$q = -R_g \left[\frac{\partial \ln p_H}{\partial(1/T)}\right]_{n_t}. \qquad (22)$$

While the pressure did not extend low enough to obtain ΔH as $n_t \to 0$, the data at $n_t \approx 4.6 \times 10^{-4}$ g mole/g gave $q = 12$ kcal/g mole. This compares with 14 kcal/g mole obtained by Schuit and van Reijen (2) and 12–~15 kcal/g mole reported by

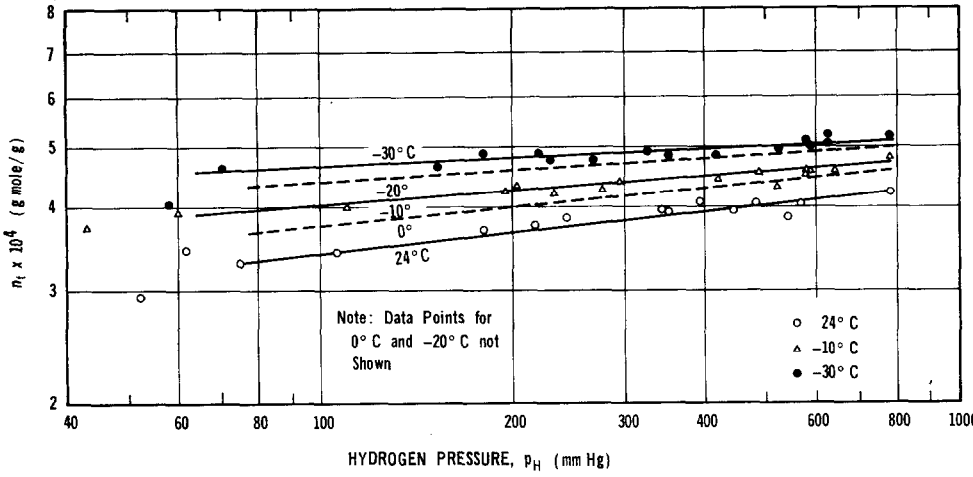

FIG. 1. Adsorption isotherms for H_2 on nickel.

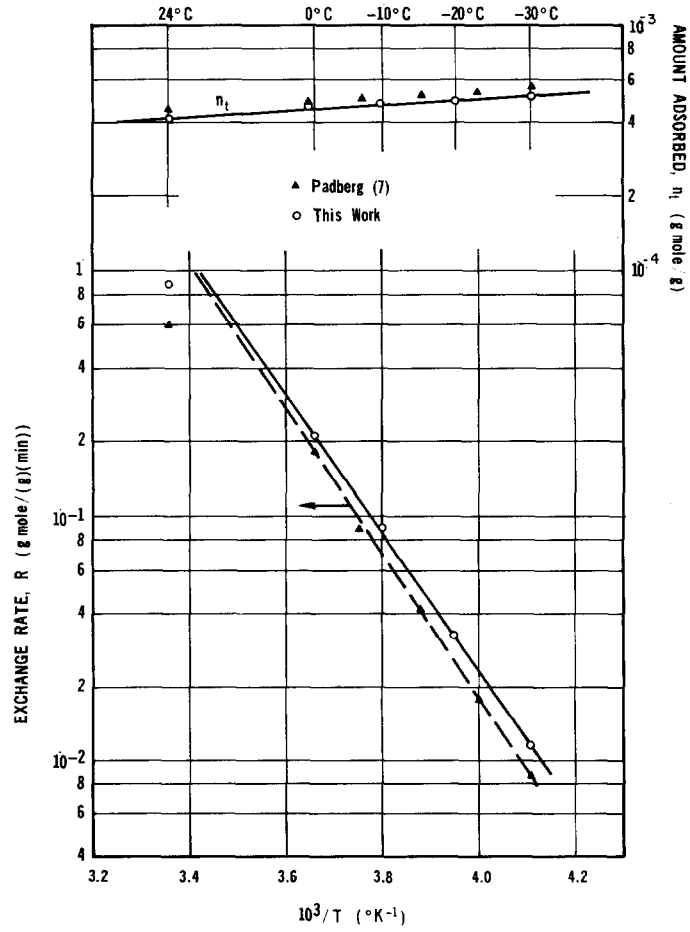

FIG. 2. Exchange rate and amount adsorbed at 780 mm Hg.

Ozaki and colleagues (*9*) for similar nickel catalysts.

Second-Moment Analysis

Effect of Transport Processes

To obtain k^* from Eq. (21), δ_1 must first be calculated. Since δ_0 (and K^*) is known from the analysis of the first moments, δ_1 can be found using Eq. (19), provided H_0 is known. The second-moment data give H, from which H_0 can be obtained from Eq. (18) by subtracting the axial dispersion contribution, $E_A/(\alpha v^2)$. The latter contribution was first evaluated by plotting the helium-pulse data as H vs $1/v$, as shown in the lowest curve in Fig. 4a. Extrapolation to $1/v = 0$ gave $H_0 \approx 0.2 \times 10^{-5}$ min. Subtracting this value of H_0 from H at any velocity gives $H - H_0$, which is the axial dispersion contribution. The results are shown as points in Fig. 3, while the curve represents the correlation, applied to helium, recently proposed (*10*) for axial dispersion in beds of small particles. The agreement between points and curve is good. Therefore, the following equation, which represents the correlation, was used to account for axial dispersion in the deuterium moments:

$$H - H_0 = \frac{1}{v^2}\frac{E_A}{\alpha} = 0.083\,\frac{1}{v} + 0.77\,\frac{\mathfrak{D}}{v^2}. \quad (23)$$

($H - H_0$ is in minutes.)

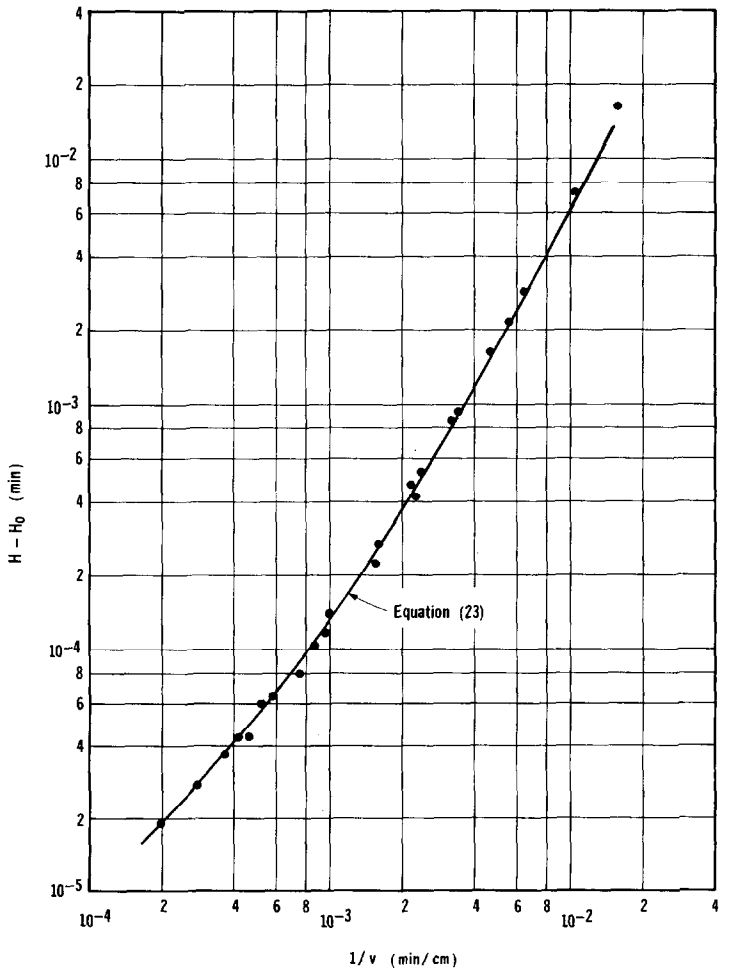

FIG. 3. Axial dispersion correction ($H - H_0$) from helium runs.

Using Eq. (23) and H obtained from the measured moments, H_0 was available for all the deuterium-pulse runs. The effect of axial dispersion on H is illustrated for the pure hydrogen (no diluent helium) data in Figs. 4a and 4b. It is seen that the intercept, H_0, is a small fraction of H at 24°C, at most velocities. Hence, at this temperature the effect of axial dispersion is very large and the accuracy of H_0 is reduced. In contrast, at —30°C the intercept is nearly as large as H so that axial dispersion has a small effect on H.

H_0 still contains the influence of mass transfer resistance ($\sim 1/k_f$) from gas to outer surface of the particles and the effect of intraparticle diffusion ($\sim 1/D_e$). As evaluated by Schneider (*8*), the gas-to-particle surface contribution to H_0 (or δ_1), as given in Eq. (21), is negligible for small particles. For the same reason the intraparticle diffusion contribution is small, but

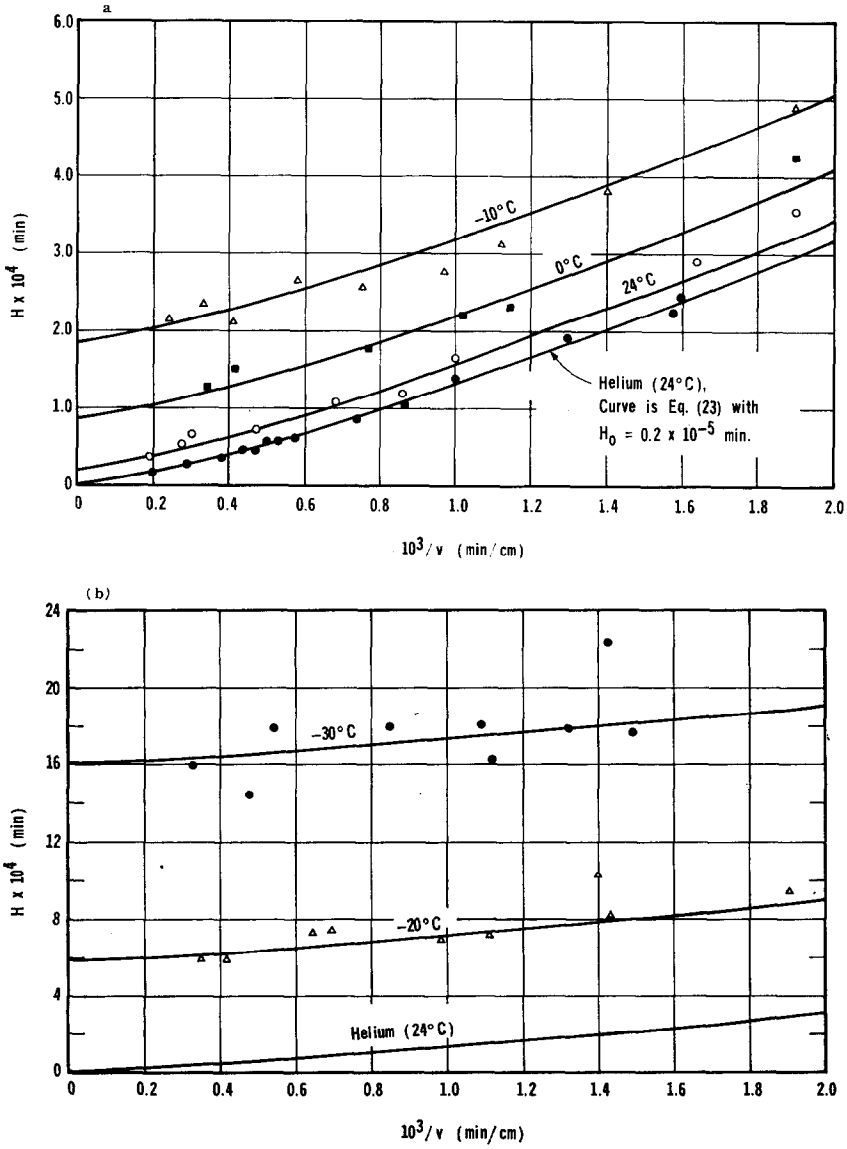

FIG. 4. (a) High-temperature deuterium data (with pure hydrogen). (b) Low-temperature deuterium data (with pure hydrogen).

not always negligible, particularly at high temperatures. The small combined effect of gas-to-particle surface mass transfer and intraparticle diffusion is confirmed from the low value of the intercept in Fig. 4a for the helium curve. Neglecting the contribution of $1/k_f$ to δ_1 and taking $K^* = 0$ for helium, Eqs. (19) and (21) may be solved for D_e to give

$$D_e = \frac{1}{15} \frac{\frac{1-\alpha}{\alpha}\beta r_0^2}{\left(1 + \frac{1-\alpha}{\alpha}\beta\right)^2} \left(\frac{1}{H_0}\right). \quad (24)$$

For $H_0 \approx 0.2 \times 10^{-5}$ min, Eq. (24) gives $D_e \approx 1.1 \times 10^{-2}$ cm^2/sec. Padberg (7) carefully established D_e for the same catalyst by measuring moments for different particle sizes and obtained $D_e = 1.25 \times 10^{-2}$ cm^2/sec. This latter value was used to account for the effect of intraparticle diffusion.

With H_0 evaluated and D_e known, Eqs. (19) and (21) were employed to obtain k^*. Thus all the transport-process effects have been accounted for.

Hydrogen Exchange Rates

The values of k^* were calculated as just described for all the deuterium-pulse data. Then R was obtained from Eq. (11). The results are plotted as R vs p_H in Fig. 5. The points at $p_H = 780$ mm for pure hydrogen represent the average of 10–14 values corresponding to different velocities. At low p_H, where R is low, and at the highest temperature, both axial dispersion and intra-

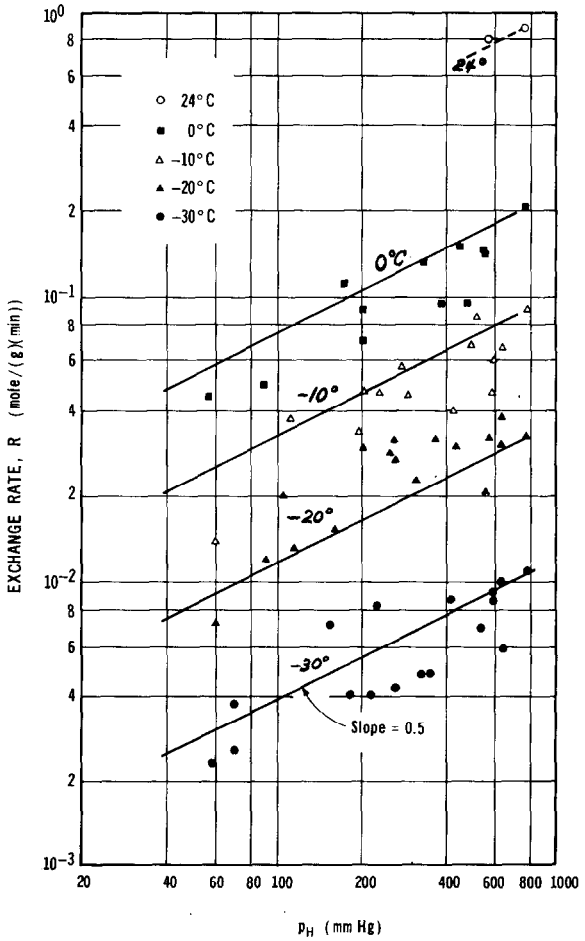

FIG. 5. Effect of hydrogen pressure on exchange rate.

particle diffusion effects are large and the accuracy of R is low. For this reason rates were not calculated at 24°C when p_H is less than 480 mm.

The rates at 780 mm are also shown in the lower part of Fig. 2 where they are compared with the results of Padberg (7). The agreement for rate measurements is reasonably good, but note that the deviations are larger than for the n_t results given in the upper part of Fig. 2. This is due to the greater sensitivity of the second moment [through the squared term in Eq. (14)] to experimental errors in the chromatographic peak.

It is the error in the second moments that leads to the scatter of the points in Fig. 5. Nevertheless, the results show that the rate increases with p_H, even though the change in n_t (Fig. 1) with hydrogen pressure is small.

Kinetics of Exchange Rate

The data in Figs. 1 and 5 are the major results of this investigation. From Fig. 5 the order of R with respect to hydrogen pressure is about 0.5, in agreement with mechanism III [Eq. (8)]. Because of the possible complexities mentioned earlier in the interaction of hydrogen with nickel surfaces, it is not wholly rewarding to relate the results to the ideal effects of p_H as represented by Eqs. (6–8). It may be that all three mechanisms occur simultaneously with magnitudes such that the composite R shows a half-power dependency of p_H. Alternatively, mechanism I may predominate but heterogeneities in sites, and/or ad-

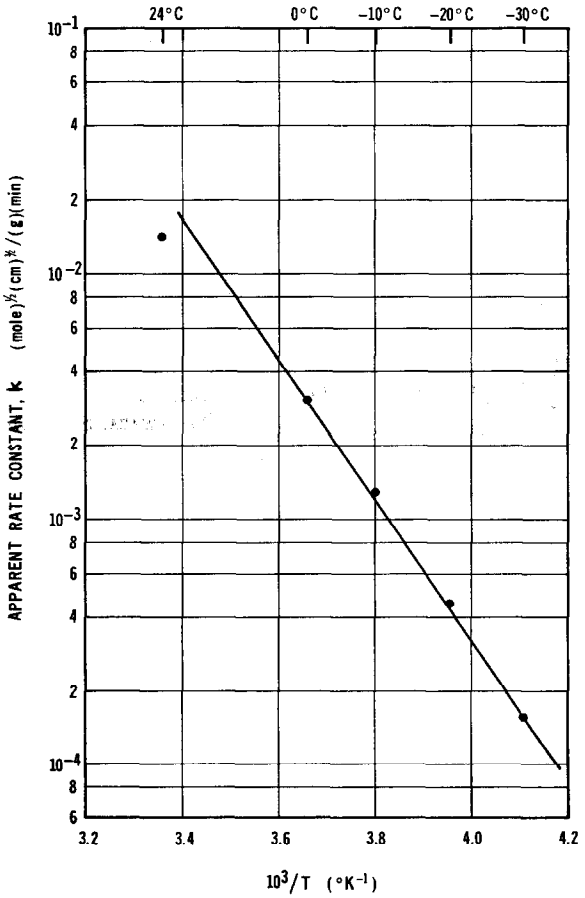

FIG. 6. Arrhenius plot of apparent rate constant.

sorbed hydrogen, possibly could cause deviations from the zero-order effect predicted by Eq. (6).

Regardless of the uncertainity about mechanism, an apparent rate constant k can be evaluated from the data in Fig. 5 using the empirical expression

$$R = k(C_H)^{1/2} = k\left(\frac{p_H}{R_g T}\right)^{1/2}. \quad (25)$$

The values of k calculated from the data in Fig. 5 are plotted vs $1/T$ in Fig. 6. Each point in Fig. 6 corresponds to the k value for the line at the corresponding temperature in Fig. 5. The slope of the line in Fig. 6 gives an apparent activation energy, E, of 13 kcal/mole. The results agree with the findings of Schuit and van Reijen (*2*). By a transient method they found E and q for a hydrogen–Ni/silica system at high-surface coverage to be 12 kcal/mole and 14 kcal/mole, respectively.

If mechanism III is the chief reason for the pressure effect shown in Fig. 5, combination of Eqs. (8) and (25) gives

$$k = k_{III}\left(\frac{R_g T}{K_e}\right)^{1/2}. \quad (26)$$

Combining this expression with the Arrhenius equation suggests that the activation energy for mechanism III would be related to E as follows:

$$E_{III} = E - \frac{1}{2}(q - R_g T). \quad (27)$$

Since $E = 13$ and $q = 12$ kcal/mole, Eq. (27) shows that $E_{III} \approx 7$ kcal/mole. This result suggests that mechanism III would be an activated process. While it would be contradictory to the data in Fig. 5, if mechanism I is dominant, Eq. (6) requires that $R = k_d = k_a/K_e$. For this rate equation the activation energy E_d also would be about 13 kcal/mole. Then $E_a = E_d - q \approx 0$. Thus, the Bonhoeffer–Farkas mechanism shows that exchange occurs by a nonactivated, adsorption process.

Acknowledgments

The financial assistance of National Science Foundation Grant GK 2243 is gratefully acknowledged. The Catalyst Division of Chemetron Corporation kindly supplied the nickel catalyst.

References

1. Beeck, O., *Advan. Catal. Relat. Subj.* **2**, 151 (1950).
2. Schuit, G. C. A., and van Reijen, L. L., *Advan. Catal. Relat. Subj.* **10**, 242 (1958).
3. Halpern, J., *Advan. Catal. Relat. Subj.* **11**, 301 (1959).
4. Bond, G. C., "Catalysis by Metals," Academic Press, New York, 1962.
5. Adrian, J. C., and Smith, J. M., *J. of Catal.* **18**, 57 (1970).
6. Suzuki, M., and Smith, J. M., *J. Catal.* (in press).
7. Padberg, G., and Smith, J. M., *J. Catal.* **12**, 172 (1968).
8. Schneider, P., and Smith, J. M., *AIChE J.* **14**, 762 (1968).
9. Ozaki, A., Nozaki, F., Maruya, K., and Ogasawara, S., *J. Catal.* **7**, 234 (1967).
10. Suzuki, M., and Smith, J. M., *The Chem. Eng. J.* (in press).